

Dyons near the transition temperature in $SU(3)$ lattice gluodynamics

V. G. Bornyakov

*Institute for High Energy Physics NRC “Kurchatov Institute”, 142281 Protvino, Russia,
Institute of Theoretical and Experimental Physics, 117259 Moscow, Russia
School of Biomedicine, Far East Federal University, 690950 Vladivostok, Russia*

E.-M. Ilgenfritz

Joint Institute for Nuclear Research, BLTP, 141980 Dubna, Russia

B. V. Martemyanov

*Institute of Theoretical and Experimental Physics, 117259 Moscow, Russia
National Research Nuclear University MEPhI, 115409, Moscow, Russia
Moscow Institute of Physics and Technology, 141700, Dolgoprudny, Moscow Region, Russia*

(Dated: May 26, 2022)

We study the topological structure of $SU(3)$ lattice gluodynamics by cluster analysis. This methodological study is meant as preparation for full QCD. The topological charge density is becoming visible in the process of overimproved gradient flow, which is monitored by means of the the Inverse Participation Ratio (IPR). The flow is stopped at the moment when calorons dissociate into dyons due to the overimproved character of the underlying action. This gives the possibility to simultaneously detect all three dyonic constituents of KvBLL calorons in the gluonic field. The behaviour of the average Polyakov loop under (overimproved) gradient flow could be also (as its value) a diagnostics for the actual phase the configuration is belonging to. Timelike Abelian monopole currents and specific patterns of the local Polyakov loop are correlated with the topological clusters.

The spectrum of reconstructed cluster charges Q_{cl} corresponds to the phases. It is scattered around $Q_{cl} \approx \pm 1/3$ in the confined phase, whereas it is $Q_{cl} \approx \pm 0.6 \div 0.7$ for heavy dyons and $|Q_{cl}| < 0.3$ for light dyons in the deconfined phase. Heavy dyons are increasingly suppressed with increasing temperature.

The paper is dedicated to the memory of Michael Müller-Preussker who was a member of our research group for more than twenty years.

PACS numbers: 11.15.Ha, 12.38.Gc, 12.38.Aw

Keywords: Lattice gauge theory, caloron, dyon

I. INTRODUCTION

There are topological objects in the vacuum of Yang Mills theory and QCD (at finite temperature) known as constituent “dyons” of Kraan-van Baal-Lee-Lu (KvBLL) calorons [1–3]. These objects have been studied for a long time in $SU(2)$ and $SU(3)$ gluodynamics and then in QCD both in the confined and deconfined phases [4–8]. The fermionic topological charge density constructed from low lying modes of the overlap Dirac operator (for two or three types of temporal boundary conditions imposed to the fermion field) was more recently used for this goal. Methods connected to the spectrum of the overlap Dirac operator are rather computer time intensive, such that we recollect here, first for the example of pure gluodynamics, how much information in this respect can be obtained by means of purely gluonic observables: the gluonic topological charge density, the Polyakov loop (global and local) and Abelian monopoles (obtained in the Maximal Abelian Gauge). Many of these tools have been proposed and used by us occasionally in the past.

The main problem with the gluonic topological charge density is that it is too noisy in vacuum glu-

onic fields (in Monte Carlo or Hybrid Monte Carlo ensembles) such that a topological structure is not discernible. The objects we are looking for (calorons, dissociated or not dissociated into dyons) appear only in the process of cooling or its continuous analog - the gradient flow [9–11], usually realized with respect to the Wilson action (therefore Wilson flow). The gradient flow with respect to so-called over-improved action [12] has an additional built-in feature of forced dissociation of calorons into dyons [13]. This is an advantage if we want to analyze the gauge field configurations down to the caloron-constituents - the dyons. During this process, the dissociation of calorons can be controlled by monitoring the inverse participation ratio (IPR) of the modulus $|q(x)|$ of the topological charge density. This IPR varies between the extreme situations $\text{IPR} = 1$ (for a homogeneously delocalized density) and $\text{IPR} = V_4$ (for a pointlike localized density). V_4 is the four dimensional volume. The IPR is defined (analogously to the IPR of the scalar density $|\psi(x)|^2$ of fermionic modes) as follows:

$$\text{IPR} = V_4 \frac{\sum_x |q(x)|^2}{(\sum_x |q(x)|)^2} . \quad (1)$$

The IPR increases while perturbative fluctuations of

the gluonic field are removed, also while already existing structures are removed by annihilation (like calorons and anticalorons as well as their dyon and antidyon constituents). Only the dissociation of calorons into dyons leads to a decrease of the IPR. So, we are in the position to stop the process of over-improved gradient flow (monitoring the IPR) when calorons are maximally delocalized (dissociated to dyons). As a rule, the IPR of a given configuration first grows to a maximum. Then it decreases before it grows again.

Maximal delocalization should happen (approximately) at the first minimum after the first maximum of the IPR in the over-improved gradient flow history. In practice we used a fixed flow time for all flow histories (at the same temperature) when they typically go through the above mentioned minimum.

II. THERMAL ENSEMBLES

For this methodical study of dyon detection in $SU(3)$ gauge theory we employ quenched ensembles which are easily created by means of the standard Wilson action S_W with the lattice coupling $\beta = 6/g_0^2$.

To fix the corresponding lattice spacing a as a function of β for this action we rely on the Necco–Sommer parametrization [14].

The test ensembles (to describe three temperatures) consist of asymmetric lattices with a four-dimensional volume $V_4 = a^4 L_t \cdot L_s^3$, where $L_t = 6$ is the number of sites in the temporal direction, and $L_s = 24$ the size in all spatial directions. The phase transition for these lattice sizes takes place at $\beta_c = 5.894$ [15]. It corresponds to a critical temperature of pure gluodynamics $T_c \simeq 300$ MeV [16].

Our test ensembles (100 configurations each) for the three temperatures of interest, $T = 0.79 T_c$, $T = 1.27 T_c$ and $T = 1.5 T_c$, are generated with $\beta = 5.8$, $\beta = 6.0$ and $\beta = 6.084$, respectively.

III. FLOW HISTORIES

For illustration, over-improved gradient flow histories are shown for 12 configurations out of each test ensemble, below and above T_c ($T = 0.79 T_c$ and $T = 1.27 T_c$), respectively, in Fig. 1 and Fig. 2. The figures show in parallel the localization of the topological density IPR, the total topological charge Q , and the action in instanton units (from top to bottom) and on Fig. 3 the volume-averaged Polyakov loop (PL). In all cases 600 steps (with step length $\epsilon = 0.02$) of flow are shown.

The flow histories for the volume-averaged Polyakov loop (PL) are different in the confining and deconfining phases: while in the confining phase PL has no preferred direction of evolution (interpreted in [17] as the result of an equal number of dyons of all three

types), in the deconfining phase PL goes in the direction where rare heavy dyons – left from supposedly asymmetric caloron solutions – become more and more heavy, whereas more abundant light dyons become more and more light (also this interpretation was given in [17]).

The flow histories for the topological charge show very fast stabilization towards integer topological charges (for our lattices up to $Q = \pm 8$) in the confining phase and towards $Q = 0$ or $Q = \pm 1$ in the deconfining phase. In the confining phase, IPRs first grows, then decreases until – at several hundreds of flow steps – it goes through a local minimum, before finally it grows again. In the deconfining phase, IPRs always monotonously grows, at least for $Q = \pm 1$. For $Q = 0$ configurations, the IPR experiences no sizable changes under gradient flow. In all cases, the action monotonously decreases, although it most rapidly does so at $T > T_c$.

Like in our previous paper [17], we will interpret also the IPR flow histories in terms of a dyonic picture. The growth of IPR in the confined phase can be understood as result of the removal of perturbative fluctuations and of the decreasing number of separate topological objects in the process of annihilation of calorons and anticalorons (as well as of their constituent dyons and antidyons). The topological charge density becomes more localized when perturbative fluctuations are hidden under the peaks of the topological charge density of topological objects. The subsequent drop of IPR we may interpret as the result of an increasing number of separate topological objects in the process of dissociation of calorons into constituent dyons. Thus, the first minimum (after passing the first maximum) in the history curve of IPR can be considered as a point of maximal dissociation of calorons to dyons in the course of over-improved gradient flow. We believe, it is a good choice to stop the flow process here for the observation of these dyons. As it can be seen from Fig. 1 for IPR, in the confined phase several hundreds of flow steps is needed to reach this point. In practise we used 600 steps to be sure that maximal dissociation has been achieved for all confining configurations.

In the deconfined phase, the topological objects expected are heavy dyons with highly localized and high-valued topological charge density on one hand and light dyons with delocalized and low-valued topological charge density on the other. The calorons are expected to be already dissociated into these asymmetric kinds of dyons. For $Q = 0$ configurations in the deconfined phase we have no heavy dyons, and the $IPR \approx 2$ will experience no sizable changes during the flow process. For $Q = \pm 1$, the final IPR is defined (after removal of perturbative fluctuations) by a single heavy dyon with highly localized charge density and its absolute topological charge being close to one.

Since we have no stopping criterium for the decon-

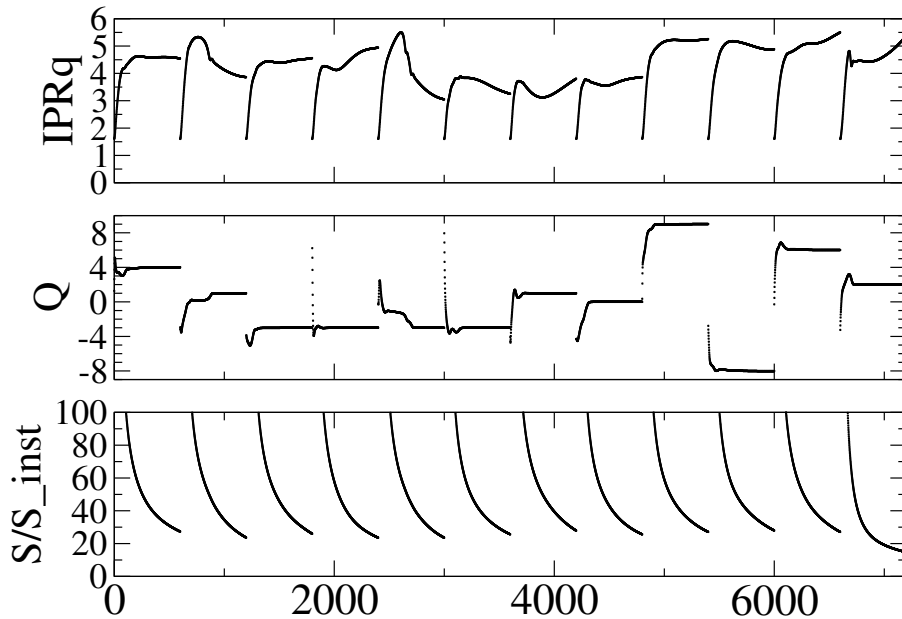


FIG. 1: Over-improved flow histories for 12 configurations below T_c ($T = 0.79 T_c$) shown for IPR, the topological charge Q and the action in instanton units (from top to bottom).

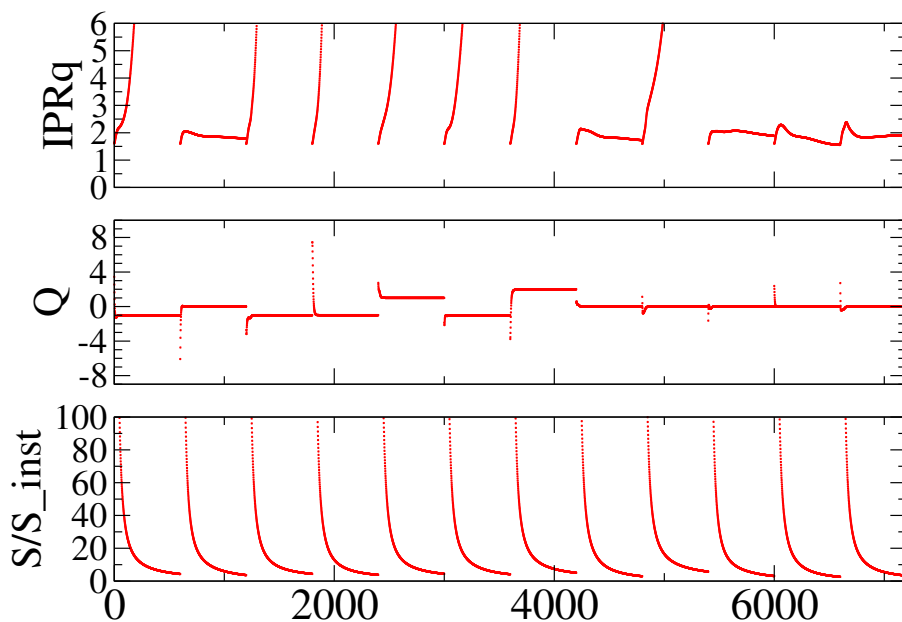


FIG. 2: Over-improved flow histories for 12 configurations below T_c ($T = 1.27 T_c$) shown for IPR, the topological charge Q and the action in instanton units (from top to bottom).

finer phase that would be motivated by the IPR history (opposite to the confined phase) we finish the flow process after approximately 100 steps of gradient flow when the actions of a configuration are comparable to those after 600 steps of flow in the confined phase .

IV. CORRELATION BETWEEN ABELIAN MONOPOLES AND POLYAKOV LINES IN AFTER-FLOW GLUON FIELDS

Relatively isolated dyons in KvBLL caloron solutions are monopoles, and the local holonomies (untraced Polyakov lines) have the specific property that two eigenvalues of the holonomy become degenerate there [18]. In the case of $SU(2)$ gauge theory this cor-

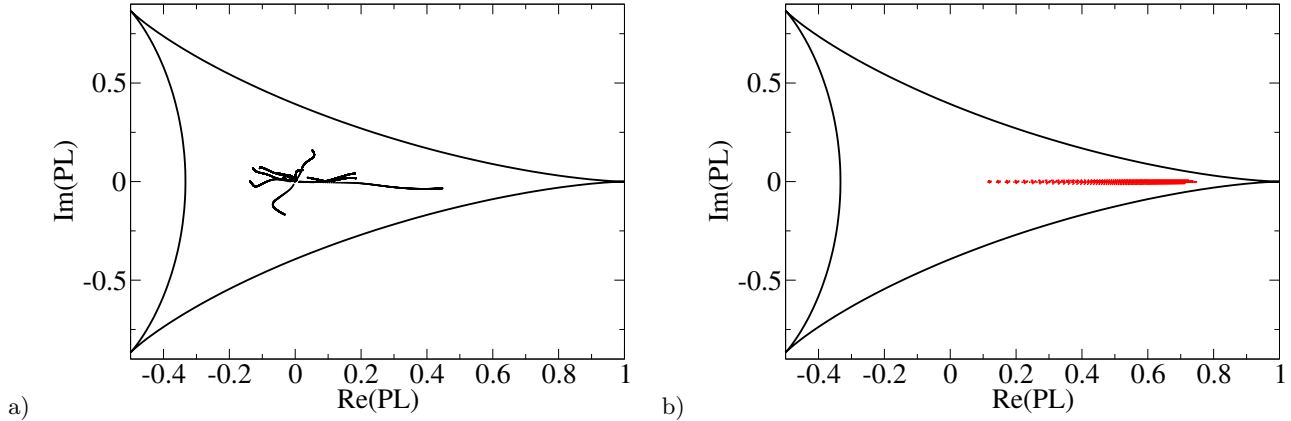


FIG. 3: Over-improved flow histories of the volume-averaged Polyakov loop for 12 configurations below/above T_c : (a) at $T = 0.79 T_c$ and (b) at $T = 1.27 T_c$, respectively.

responds to the points where Polyakov lines take the values $\pm I$. Abelian monopoles (in the sense of Abelian projection of MAG) and dyon constituents of KvBLL caloron solution (placed on the lattice) are in one-to-one correspondence (at least for isolated objects), and in the $SU(2)$ case they are correlated with the above mentioned points [19, 20].

In the $SU(3)$ case the degeneracy of Polyakov lines corresponds to the flanks of the unitarity triangle [18]. For a Polyakov line

$$\text{diag}(e^{2\pi i\mu_1}, e^{2\pi i\mu_2}, e^{2\pi i\mu_3})$$

(with $\mu_1 \leq \mu_2 \leq \mu_3 \leq \mu_4 = 1 + \mu_1$ and $\mu_1 + \mu_2 + \mu_3 = 0$) parametrised by three numbers $m_1 = \mu_2 - \mu_1$, $m_2 = \mu_3 - \mu_2$ and $m_3 = \mu_4 - \mu_3$ this degeneracy happens when either m_1 or m_2 or m_3 vanish.

The inter-correlation of Abelian monopoles and the monopoles defined by degenerated eigenvalues of holonomy lines can be detected by a correlation between loci of minimum of m_1 , m_2 , m_3 with Abelian monopoles localized in MAG [8]. Which one of m_1 , m_2 or m_3 becomes very small determines the type of dyon. On Fig. 4 the distributions of $\min(m_1(x), m_2(x), m_3(x))$ taken over all lattice sites (shaded histogram) is compared with the distribution over all cubes which are duals of time-like monopole links (open red histogram). The latter are loci where thermal monopoles are located. This is shown for $T = 0.79 T_c$ in the confined phase (Fig. 4 a) and for $T = 1.27 T_c$ in the deconfined phase (Fig. 4 b). In the case of a monopole the minimum $\min(m_1(x), m_2(x), m_3(x))$ is taken over the eight corners of the three-dimensional cube containing that monopole. It is seen that the distribution of $\min(m_1(x), m_2(x), m_3(x))$ on thermal monopoles is shifted towards zero compared with the distribution in the bulk. It is also seen that in the deconfined phase,

when the Polyakov loop in the bulk (holonomy) moves towards the corners of the unitarity triangle ((1,0) in our case) light dyons are heavily seen having their Polyakov loops in the bulk Polyakov loop profile.

V. CLUSTER ANALYSIS

Having access to the topological charge density at all lattice points at a selected time of the gradient flow, allows to perform a cluster analysis of the topological density, expecting to be able to associate the emerging clusters with dyons. The method of the analysis was described many times, for example in [8]. As it can be seen from table I, clusters occupy several percent of the lattice volume (equal to 26 fm^4 , 5 fm^4 , 2.5 fm^4 for ensembles at temperatures $T = 0.79 T_c$, $T = 1.27 T_c$, $T = 1.5 T_c$, respectively) and are correlated to magnetic monopoles. The correlation is strongest in the confined phase.

We see that at $T = 0.79 T_c < T_c$ approximately 100 (from around 300 in total) of dual time-like links carrying monopole currents are concentrated in only 2.4% of the lattice occupied by topological clusters. On the other hand the remaining approximately 200 of dual time-like links carrying monopole currents are spreaded over 97.6% of the rest of the lattice. Thus, time-like Abelian magnetic currents are about 20 times more dense inside clusters of topological charge than outside. Also, in this phase around 10 clusters containing time-like magnetic monopoles at all, are pierced totally by around $20 = 2 \times 10$ time-like magnetic current loops (of thermal monopoles) as it should be for a KvBLL dyon. This is because each dyon is a monopole in one Abelian field and an antimonopole in another Abelian field, for the three

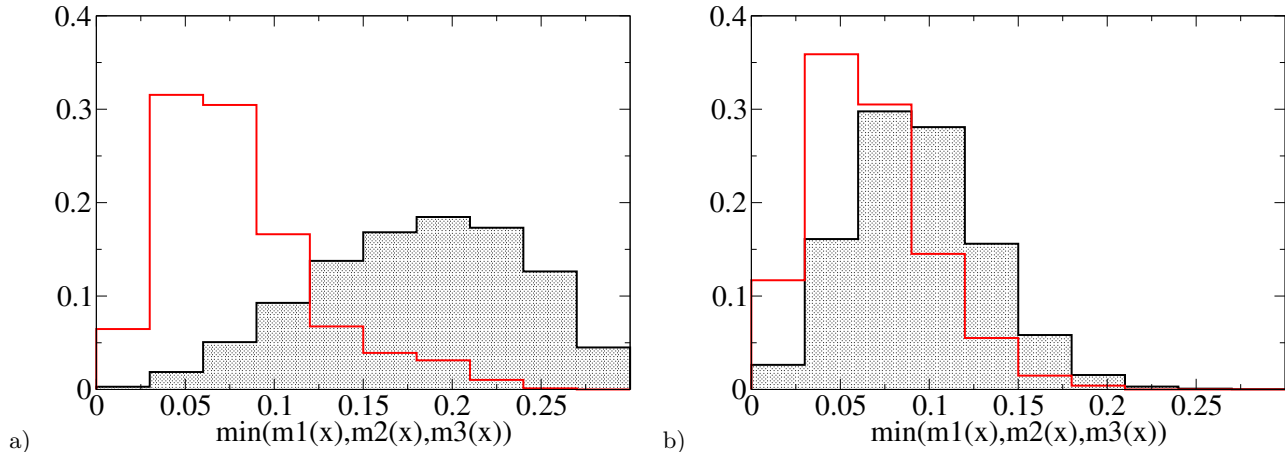


FIG. 4: The distributions with respect to the minimal distance $\min(m_1(x), m_2(x), m_3(x))$ between the local Polyakov loop value and the nearest flank of the Polyakov triangle over all lattice sites (shaded histogram) and for all cubes where thermal monopoles are located (open red histogram) are shown in (a) for $T = 0.79 T_c$ in the confined phase and in (b) for $T = 1.27 T_c$ in the deconfined phase.

phase	V_{cl}	V_{clmon}	N_{cl}	N_{clmon}	N_{mon}	N_{moncl}	N_{loop}	N_{loopcl}
$T = 0.79 T_c < T_c$	2.6(1)%	2.4(1)%	15.4(2)	10.4(2)	306(6)	94(3)	45(1)	19(1)
$T = 1.27 T_c > T_c$	2.7(3)%	1.0(1)%	29(2)	3.0(2)	130(3)	21(2)	21(1)	5.2(4)
$T = 1.5 T_c > T_c$	4.7(3)%	1.2(1)%	45(2)	3.0(2)	106(3)	19(1)	18(1)	5.9(4)

TABLE I: Results of the cluster analysis. All numbers indicate averages per configuration. The pure statistical errors are given in parentheses. We denote with V_{cl} - the volume fraction occupied by all topological clusters, V_{clmon} - the volume fraction occupied by clusters containing time-like magnetic monopoles, N_{cl} - the number of all clusters per configuration, N_{clmon} - the number of clusters containing time-like magnetic monopoles, N_{mon} - the overall number of dual time-like links carrying monopole currents, N_{moncl} - the number of dual time-like links with monopole currents found inside topological clusters, N_{loop} - the overall number of thermal monopoles (closed in time direction magnetic current loops), N_{loopcl} - the number of these thermal monopoles piercing topological clusters.

Abelian fields available in the case of $SU(3)$.

The (reconstructed) topological charges (Q_{cl}) of the clusters containing time-like magnetic monopoles are distributed around $\pm 1/3$ in the confined phase (see Fig. 5b)). In the deconfined phase, these clusters form two groups, one of heavy clusters with $|Q| > 0.6 \div 0.7$ on one hand and another of light clusters with $|Q| < 0.3$ (see Fig. 6b)) on the other hand.

The “reconstructed” cluster charge is obtained by summing over the charge density according to a procedure described in [8, 19, 20], where also the systematic error is estimated. Finally, in the confined phase, the trace of the Polyakov line measured inside the clusters in representative points (where the minimum $\min(m_1(x), m_2(x), m_3(x))$ is taken on) is indeed located closeby to the flanks of the Polyakov triangle. This is an expected feature of KvBLL monopole-dyons appearing in three types (of approximately equal charge and abundance) in the confined phase (see Fig. 5a)). The three flanks correspond to the

three types of dyon observed.

phase	$\rho_3(1)$	$\rho_3(2)$	$\rho_3(3)$
$T = 0.79 T_c < T_c$	1.22(2)	1.22(2)	1.22(2)
$T = 1.27 T_c > T_c$	1.15(7)	1.35(7)	1.35(7)
$T = 1.5 T_c > T_c$	0.54(4)	3.1(2)	3.1(2)

TABLE II: 3-dim densities $\rho_3(i)$, $i = 1, 2, 3$ for heavy, light, light dyons at all three temperatures in $1/\text{fm}^3$ units.

In the deconfined phase, the position of heavy and light clusters (represented by the trace of the Polyakov line) in the Polyakov triangle is indicated by points with $\min(m_3(x))$ or $\min(m_1(x), m_2(x))$ for heavy or light clusters (see Fig. 6a)), respectively. We see that 11 out of 38 clusters found in (totally) 12 configurations are heavy so that heavy dyons are relatively

suppressed with respect to the light ones. This is also an expected feature of KvBLL monopole-dyons. Finally, we can calculate 3-dim densities for dyons at all three temperatures (for dyons as static objects 3-dim densities are more relevant than 4-dim densities) The suppression of heavy dyons with the increase of temperature is clearly seen (see Table II).

VI. CONCLUSION

We have studied the topological structure of $SU(3)$ gluodynamics by cluster analysis of the gluonic topological density. The gluonic topological charge density was emerging in the process of gradient flow with respect to the over-improved action. Monitoring the IPR of the modulus of the topological density has

allowed us to stop the gradient flow at the moment when calorons have dissociated into dyons due to over-improved character of this process. This has given us the possibility to visualize all three dyon constituents of a KvBLL caloron formed in the gluonic field. The time-like Abelian monopoles and the specific KvBLL pattern of the local holonomy (untraced Polyakov line) are correlated to topological clusters. The reconstructed (summed) values of topological charges for each dyons are concentrated near $1/3$ in the confined phase. In the deconfined phase, however, the values of the cluster charges (characterizing heavy and light dyons) have been found correlated to the local holonomy. The suppression of heavy dyons with the increase of temperature is clearly seen.

Acknowledgments

B.V.M. appreciates the support by the grants RFBR 15-02-07596a, 16-02-01146a.

-
- [1] T. C. Kraan and P. van Baal, Nucl.Phys. **B533**, 627 (1998), hep-th/9805168.
 - [2] T. C. Kraan and P. van Baal, Phys.Lett. **B435**, 389 (1998), hep-th/9806034.
 - [3] K.-M. Lee and C.-H. Lu, Phys.Rev. **D58**, 025011 (1998), hep-th/9802108.
 - [4] V. Bornyakov, E.-M. Ilgenfritz, B. Martemyanov, S. Morozov, M. Müller-Preussker, and A. Veselov, Phys.Rev. **D76**, 054505 (2007), 0706.4206.
 - [5] V. Bornyakov, E.-M. Ilgenfritz, B. Martemyanov, and M. Müller-Preussker, Phys.Rev. **D79**, 034506 (2009), 0809.2142.
 - [6] E.-M. Ilgenfritz, B. Martemyanov, and M. Müller-Preussker, Phys.Rev. **D89**, 054503 (2014), 1309.7850.
 - [7] V. G. Bornyakov, E. M. Ilgenfritz, B. V. Martemyanov, and M. Müller-Preussker, Phys. Rev. **D91**, 074505 (2015), 1410.4632.
 - [8] V. G. Bornyakov, E. M. Ilgenfritz, B. V. Martemyanov, and M. Müller-Preussker, Phys. Rev. **D93**, 074508 (2016), 1512.03217.
 - [9] M. Luscher, Commun. Math. Phys. **293**, 899 (2010), 0907.5491.
 - [10] M. Lüscher, JHEP **1008**, 071 (2010), 1006.4518.
 - [11] M. Luscher and P. Weisz, JHEP **02**, 051 (2011), 1101.0963.
 - [12] M. Garcia Perez, A. Gonzalez-Arroyo, J. R. Snippe, and P. van Baal, Nucl.Phys. **B413**, 535 (1994), hep-lat/9309009.
 - [13] F. Bruckmann, E.-M. Ilgenfritz, B. Martemyanov, and P. van Baal, Phys.Rev. **D70**, 105013 (2004), hep-lat/0408004.
 - [14] S. Necco and R. Sommer, Phys.Lett. **B523**, 135 (2001), hep-ph/0109093.
 - [15] Y. Iwasaki, K. Kanaya, T. Yoshie, T. Hoshino, T. Shirakawa, Y. Oyanagi, S. Ichii, and T. Kawai, Phys. Rev. **D46**, 4657 (1992).
 - [16] C. Gattringer, R. Hoffmann, and S. Schaefer, Phys.Lett. **B535**, 358 (2002), hep-lat/0203013.
 - [17] V. Bornyakov, E.-M. Ilgenfritz, B. Martemyanov, V. Mitrjushkin, and M. Müller-Preussker, Phys.Rev. **D87**, 114508 (2013), 1304.0935.
 - [18] P. Van Baal, Nucl. Phys. Proc. Suppl. **106**, 586 (2002), hep-lat/0108027.
 - [19] E.-M. Ilgenfritz, B. Martemyanov, M. Müller-Preussker, and A. Veselov, Phys.Rev. **D71**, 034505 (2005), hep-lat/0412028.
 - [20] E.-M. Ilgenfritz, B. Martemyanov, M. Müller-Preussker, and A. Veselov, Phys.Rev. **D73**, 094509 (2006), hep-lat/0602002.

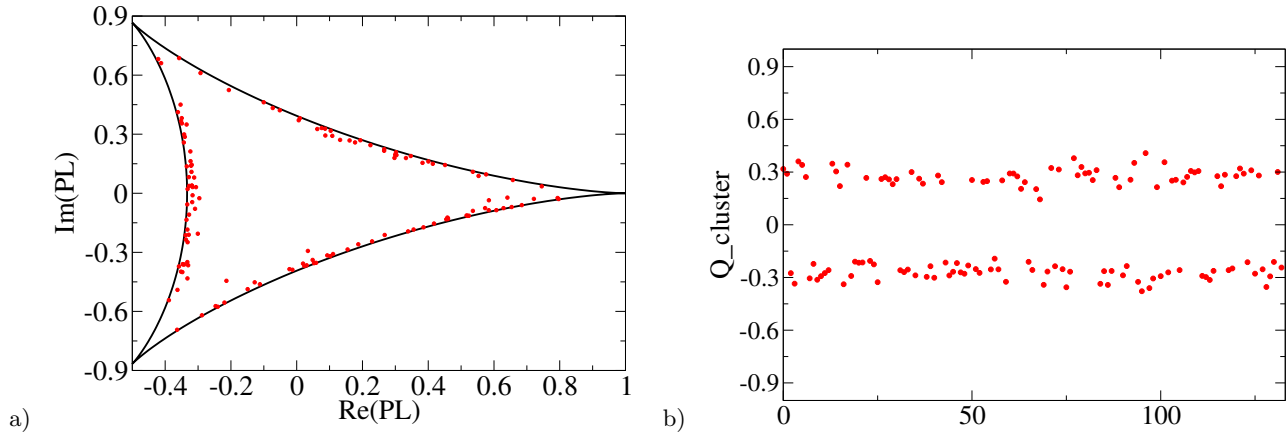


FIG. 5: a) Scatter plot of the Polyakov loop in points with $\min(m_1(x), m_2(x), m_3(x))$ for clusters in the confined phase at $T = 0.79 T_c$ (shown as circles, only clusters containing time-like magnetic monopoles are shown), b) integrated topological charges of these clusters shown also by circles. Abscissa here shows the number of cluster and for 12 presented configurations there are $10.4 * 12 \approx 125$ such clusters.

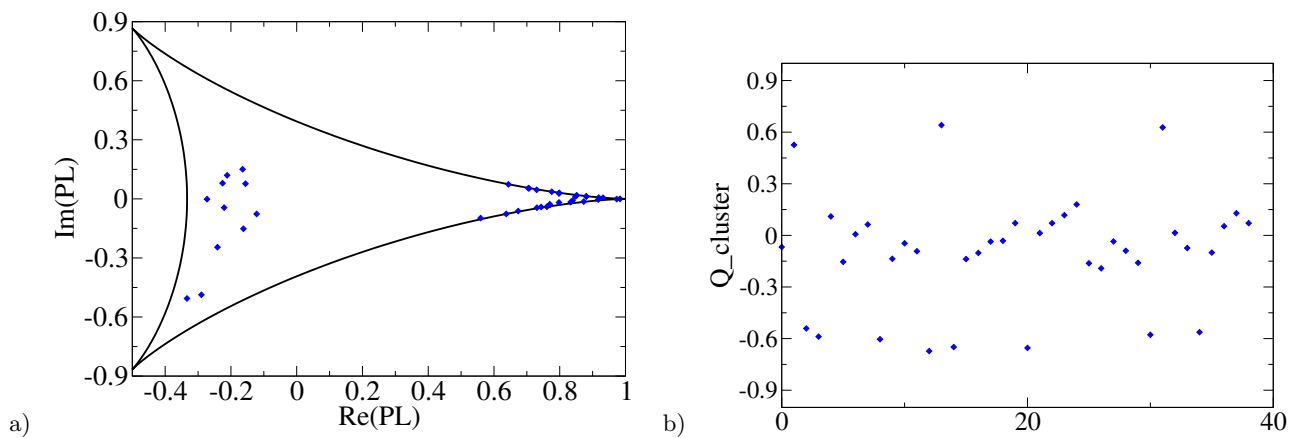


FIG. 6: a) Scatter plot of the Polyakov loop in points with $\min(m_1(x), m_2(x), m_3(x))$ for clusters in the deconfined phase at $T = 1.27 T_c$ (shown as diamonds, only clusters containing time-like magnetic monopoles are shown), b) integrated topological charges of these clusters shown also by diamonds. Abscissa here shows the number of cluster and for 12 presented configurations there are $3.2 * 12 \approx 38$ such clusters.